applied optics

Two particle tracking and detection in a single Gaussian beam optical trap

P. Praveen,[1] Yogesha,[2] Shruthi S. Iyengar,[1] Sarbari Bhattacharya,[1] and Sharath Ananthamurthy[1,*]

[1]Department of Physics, Bangalore University, Bangalore 560056, India
[2]Department of Physics, Government Science College, Hassan 573204, India
*Corresponding author: asharath@gmail.com

Received 19 August 2015; revised 5 December 2015; accepted 7 December 2015; posted 7 December 2015 (Doc. ID 248058); published 19 January 2016

We have studied in detail the situation wherein two microbeads are trapped axially in a single-beam Gaussian intensity profile optical trap. We find that the corner frequency extracted from a power spectral density analysis of intensity fluctuations recorded on a quadrant photodetector (QPD) is dependent on the detection scheme. Using forward- and backscattering detection schemes with single and two laser wavelengths along with computer simulations, we conclude that fluctuations detected in backscattering bear true position information of the bead encountered first in the beam propagation direction. Forward scattering, on the other hand, carries position information of both beads with substantial contribution from the bead encountered first along the beam propagation direction. Mie scattering analysis further reveals that the interference term from the scattering of the two beads contributes significantly to the signal, precluding the ability to resolve the positions of the individual beads in forward scattering. In QPD-based detection schemes, detection through backscattering, thereby, is imperative to track the true displacements of axially trapped microbeads for possible studies on light-mediated interbead interactions.

OCIS codes: (350.4855) Optical tweezers or optical manipulation; (290.1350) Backscattering; (290.2558) Forward scattering.

http://dx.doi.org/10.1364/AO.55.000585

1. INTRODUCTION

The standard quadrant photodetector (QPD) based techniques for tracking particle position with time in an optical tweezer (OT) are the methods for tracking forward scattering [1] and detection of backscattering [2]. However, these methods have been mostly used for tracking single particles in a single beam OT. In this study, we try to extend the standard QPD-based detection techniques to study microbeads trapped axially in a single-beam OT, which is a situation that can be inadvertently encountered when studying dense colloidal suspensions and can lead to erroneous estimates for a supposedly single particle trap stiffness as reported in [3].

Multiple micrometer-sized bead trapping has been observed in single-beam optical tweezers as well as in counterpropagating dual-beam radiation pressure traps [4]. It is shown that a redistribution of the incident light field by the particles in the trap dictates their arrangement with respect to the interparticle separations [5]. This is referred to as optically bound matter or optical matter [6]. Optical binding could provide a means for organizing colloidal and biological matter at the microscopic scale using light forces and possibly enable an alternate route to microfabrication.

It is, however, essential that the nature of interaction between the trapped microbeads is investigated before light-force-enabled micromanipulation can be a reliable method of microfabrication. For this to be done, it is essential to seek methods of tracking particle positions with time that are indeed representative of a single particle rather than multiple particles. The work presented here on the detection of the individual beads in an axial two-bead trap can be treated, therefore, as the essential first step toward understanding interbead interactions in an axial multibead trap.

We demonstrate with this study that the backscattered signal always bears true information of the bead encountered first in the optical path [Fig. 1], whereas the forward-scattered signal is an admixture of the fluctuations of both beads. A calculation of the electric field intensities incident on the quadrant detector from scattering off the trapped beads confirms that the contribution from two-bead interference is significant; hence, this precludes resolving the individual positions of the beads through monitoring the forward-scattering signal.

1559-128X/16/030585-10$15/0$15.00

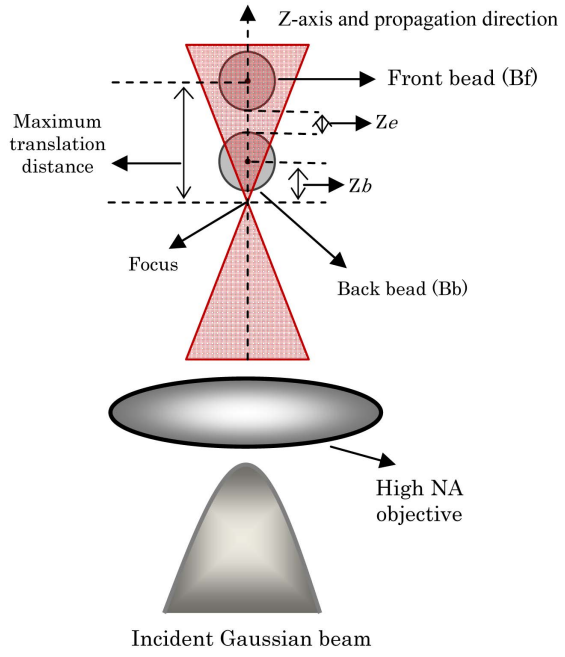

Fig. 1. Schematic for two axially trapped beads in a Gaussian beam optical tweezer. Z_b is the distance between the focus and the center of back bead; Z_e the edge-to-edge distance between the two axially trapped beads.

2. EXPERIMENTAL DETAILS

A. Single Wavelength Simultaneous Back and Forward Scattering Detection

Our optical tweezer setup consists of an Ytterbium fiber laser of wavelength 1064 nm guided into a 100× oil immersion objective with a numerical aperture (NA) of 1.4 on a custom-made inverted microscope to create the optical trap. The instrument is further equipped with an XYZ stage and QPDs for particle detection. The QPDs used for both forward- and backscattering detection are identical (H-series detectors from Electro Optical Systems, USA) and have a sensitivity of −0.0682 V/μm, and the linear region of the detector has a width of nearly 0.32 μm, which is much larger than typical fluctuations of trapped beads, which are typically tens of nanometers in size. Because, in the experiments detailed in the sections to follow, we were required to use two objectives in the oil immersion mode on either side of the sample holder, the dimensions along the beam propagation direction had to be made as small as possible. An airtight arrangement constructed using two coverslips held together by a rectangular pattern of glue was found to be an optimal sample holder that yielded good signal-to-noise ratios on both signals. Typical sample-holder depths obtained were about 10 to 20 μm with lateral dimensions of 1.5 × 3 cm.

Details of our standard OT configuration are given in [7]. For the current experiment, one of the beam paths in the setup, as described in [7], is modified as shown in Fig. 2 to enable simultaneous forward- and backscattering detection of the 1064 nm laser beam, which also is being used to trap the microbeads.

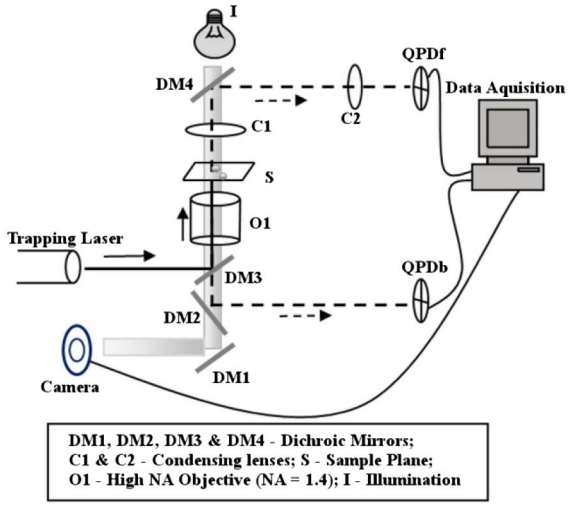

Fig. 2. Schematic of single wavelength simultaneous forward- and backscattering detection setup. Bold line indicates the incident laser light; dashed lines indicate scattered laser light.

B. Two Wavelength Simultaneous Backscattering Detection

The schematic of the setup used for this is as shown in Fig. 3(a). Unlike the earlier setup, a diode laser of 980 nm in addition to the Ytterbium fiber laser of 1064 nm and two oil-immersed objectives are used here. The objective with the higher NA of 1.4 is used for trapping with 1064 nm as in the earlier configuration. The second objective with NA of 1.25 in tandem with the 980 nm laser beam is used only for tracking the trapped beads. A 1064 nm line-pass filter and a 980 nm bandpass filter from Thorlabs, USA, are prefixed to the QPDs, as shown in Fig. 3(a), to enable detection of a backscattered signal alone on both QPDs.

For purposes of alignment, a bead was trapped using the 980 nm laser. The laser was then moved in steps of a few micrometers at a time until the center of the trapped bead coincided with the predetermined coordinates of the focal point of the 1064 nm beam. Further, careful alignment was then carried out to ensure that the 1064 and 980 nm beams were collinear. Subsequently, attenuators were introduced into the 980 nm optical path until the trap was rendered ineffective (trapped microbead escaped from the trap, and no further trapping could be observed). We also monitored the power spectra of the bead in the 980 nm trap after the introduction of each attenuator and ensured that the corner frequency after the introduction of the final attenuator was less than 3 Hz, the lower-frequency limit of our vibration isolation table. By these means, we ensured that the influence of the 980 nm laser on the trap parameters of the 1064 nm laser is negligible.

C. Two Wavelength Simultaneous Forward-Scattering Detection

The setup used to carry out this experiment is identical to that described for the two wavelength simultaneous backscattering detection except for the positions of the 1064 nm line-pass filter and the 980 nm bandpass filter. The positions of these two filters are swapped, as shown in Fig. 3(b), to enable simultaneous detection of the forward scattering alone on the two QPDs.

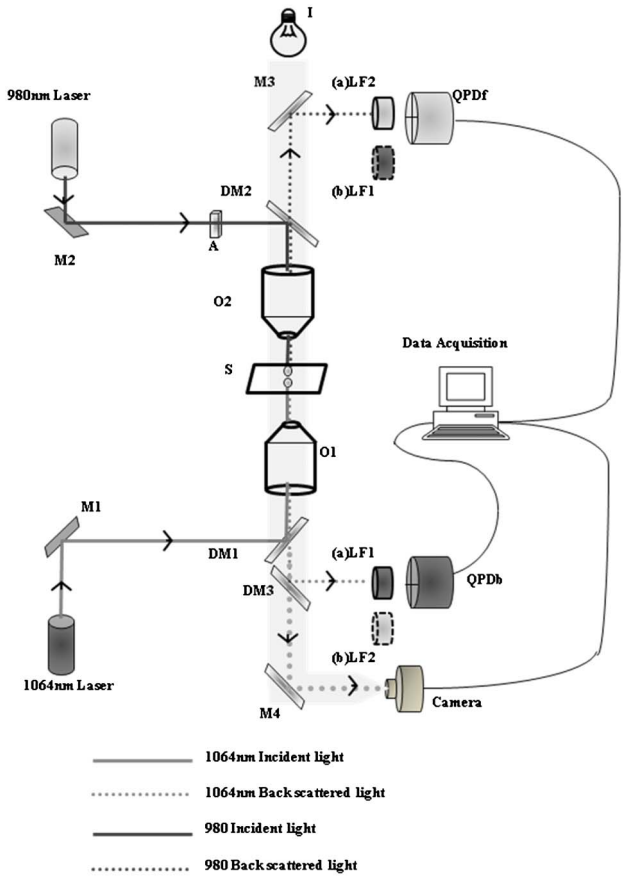

Fig. 3. (a) Schematic of two wavelength simultaneous backscattering detection setup with 1064 nm line-pass filter and 980 nm line-pass filter fixed in front of QPD*b* and QPD*f*, respectively. M1, M2, M3, and M4 are mirrors, A, attenuators; S, sample plane; I, illumination lamp; DM1 to DM3 are dichroic mirrors; O1(NA = 1.4) and O2 (NA = 1.25) are tapping and tracking objectives, respectively. LF1 and LF2 are 1064 and 980 nm line filters, respectively. (b) For two wavelengths simultaneous forward-scattering detection setup with the positions of the two line-pass filters exchanged, as shown by dotted LF1 and LF2.

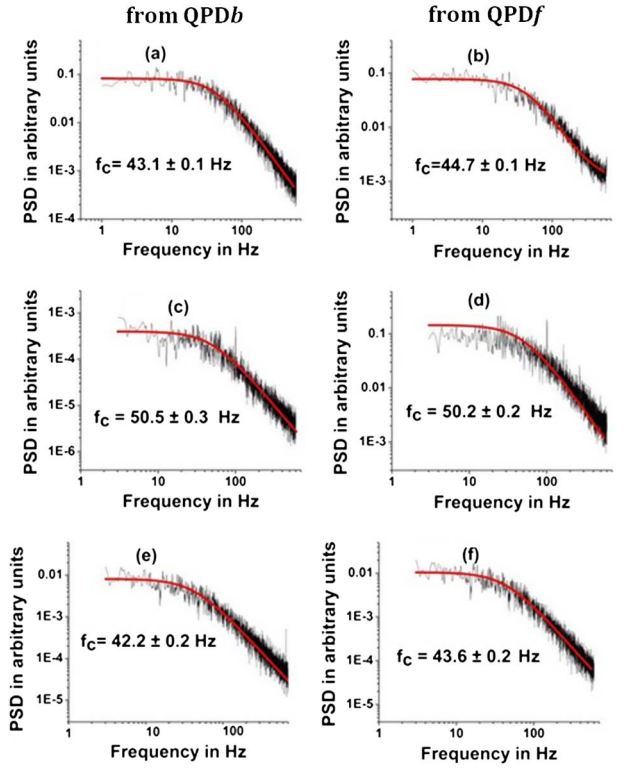

Fig. 4. PSDs obtained for a single trapped bead (a) and (b) as monitored using setup in Fig. 2; (c) and (d) as monitored using setup in Fig. 3(a); (e) and (f) as monitored using setup in Fig. 3(b).

In each of the setups in Figs. 2, 3(a), and 3(b) described above, a high frame rate camera from Point Grey Research, USA, was used to monitor and count the microbeads in the trap. Signals from the QPDs were stored on a computer hard disk and were later analyzed using codes written in LabView.

Further, in each of our setups, as shown in Figs. 2, 3(a), and 3(b), a calibration of obtaining identical corner frequencies on both QPDs for a single trapped microbead was carried out prior to any measurement involving a pair of microbeads (Fig. 4).

Throughout, we have trapped polystyrene beads with 3 μm diameter procured from Polysciences Inc., USA.

3. RESULTS AND DISCUSSION

A. Single Wavelength Simultaneous Forward- and Backscattering Detection

We trapped several pairs of beads at 600 mW and carried out simultaneous single wavelength back and forward scattering measurements. Each time, we discovered that the signals recorded on both detectors yielded modified Lorentzians in power spectral density (PSD) analysis, and the corner frequency extracted from the intensity fluctuations recorded in QPD*b* (Fig. 2, backscattering) is much larger than that from forward scattering (QPD*f*) (Fig. 2, forward scattering). In Fig. 5, we show chronologically the variation in the corner frequency as obtained from a PSD analysis of data recorded on QPD*b* when a second bead enters the trap. It may be noted that, using this detection method, it is not possible to predict where this bead will be positioned with reference to the bead already in the trap. This may depend on the initial approach condition of the second bead. However, as the beads are trapped at different axial positions, they are bound to be subjected to different trap stiffness, as reported in [3]. We find evidence of this from the increased corner frequency values, post the entrance of the second bead into the trap [Fig. 5]. We also discovered that the corner frequencies of the beads linked to any specific kind of scattering have large variation over different trials [Fig. 6(a)]. Representative data of the power spectra recorded for a pair of trapped beads using a single wavelength simultaneous forward- and backscattering detection have been shown in Fig. 6(b). This variation in corner frequencies is attributed to lack of perfect uniformity in bead size and shape as well as varying magnitude of the interbead interactions due to static charge buildup on the beads. For the case of a single trapped bead, the corner frequency extracted from the backscattering (QPD*b*) and QPD*f* detection is always almost identical and resides between the above-mentioned values (Fig. 4).

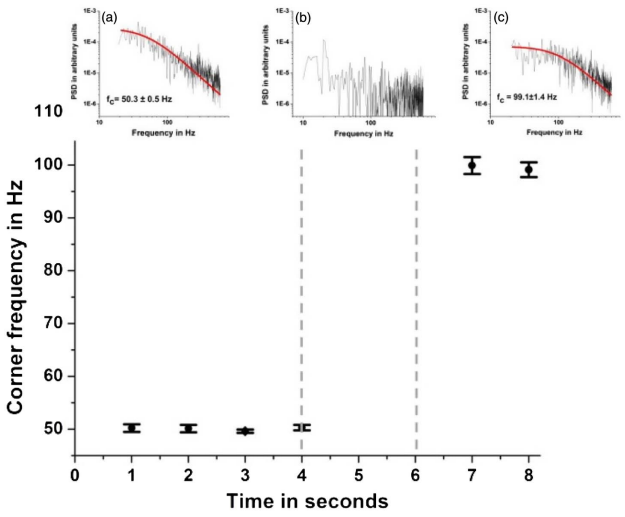

Fig. 5. Variation in the corner frequency of data recorded on QPD*b* with time as a second bead is trapped. Data logged at the end of each second is subjected to power spectral density analysis and a corner frequency with standard deviation error is reported. Insets (a) and (c) show PSDs with fits for single and double beads, respectively, where a corner frequency of 50.3 ± 0.5 Hz is obtained for the case of a single bead, while the value for the same parameter after the second bead is stably trapped is 99.1 ± 1.4 Hz. Inset (b) shows data recorded in the time period between the dashed lines where a fit to a modified Lorentzian was not possible. This is when the second bead is close enough to affect the signal detected by QPD*b* but is yet to be stably trapped.

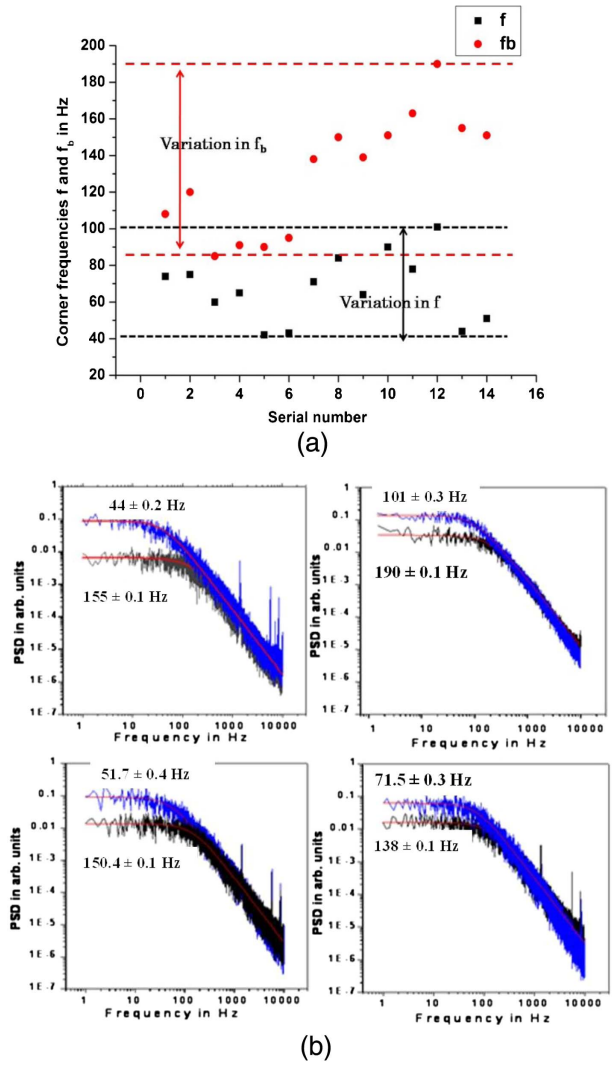

Fig. 6. (a) Plot of various corner frequencies versus trial number. Red circles, back bead corner frequency fb; black squares, effective front bead corner frequency *f*. (b) PSD plots with fits for four pairs of beads monitored using the scheme indicated in Fig. 2. PSDs extracted from fluctuations recorded on QPD*f* and QPD*b* are indicated in blue and black, respectively.

It is reasonable to assume that the bead located closer to the focal point experiences trap stiffness higher than that experienced by the other bead. Thus, we can assume that the information recorded in QPD*b* (backscattered data) is dominated by the bead located closer to the laser focal point (henceforth referred to as the back bead [Bb], Fig. 1) while the information recorded on QPD*f* is influenced by the bead located farther away from the focal point (henceforth referred to as the front bead [Bf], Fig. 1). It may be noted that, as the variation in the gradient force is rapid in regions axially closer to the focus and relatively slower in regions farther away along the propagation axis [8], one can expect to see a large increase in the corner frequency of Bb compared with the value of corner frequency for a single trapped bead. Along with a reduced gradient force owing to its larger distance from the focus, Bf also sees reduced photon flux due to the presence of Bb close to the focal region. Therefore, one can expect a much reduced corner frequency for Bf in comparison with Bb. It will be, however, impossible to understand the extent to which the fluctuation in position of the individual beads affect the information recorded in each QPD without considering, in addition, the results of the experiments on setups shown in Figs. 3(a) and 3(b), as described in the earlier section.

B. Two Wavelength Simultaneous Backscattering Detection

The experiment was carried out at laser powers of 500 and 600 mW at the source for the 1064 nm trapping laser and at 300 mW at the source for the 980 nm tracking laser. A single bead was trapped, and the backscattered signal at 1064 and 980 nm from the trapped bead was recorded simultaneously with two QPDs. The corner frequencies obtained from QPD*f* and QPD*b* were 31.5 ± 0.3 and 24.1 ± 0.2 Hz, respectively, at trapping power of 500 mW at the source and 50.5 ± 0.3 and 50.2 ± 0.2 Hz, respectively, at trapping power of 600 mW at the source for the case of the single bead (Fig. 4). The variations in the corner frequency in forward- and backscattering for a single trapped bead for each power are well within range of each other considering the signal-to-noise ratio in each of the cases.

Subsequently, a pair of beads was trapped at the abovementioned powers, and the corner frequencies of the PSDs recorded on QPD*b* and QPD*f* are tabulated in Table 1.

The power spectra recorded on QPD*b* and QPD*f* for 600 mW at the source for the 1064 nm trapping laser are

Table 1. Corner Frequencies Obtained for the Front and Back Beads Using the Setup in Fig. 3(a)

Trapping Power at the Source (in mW)	Corner Frequency (in Hz)	
	QPD*b*	QPD*f*
600	111.2 ± 0.3	32.1 ± 0.2
500	86.0 ± 0.2	23.9 ± 0.2

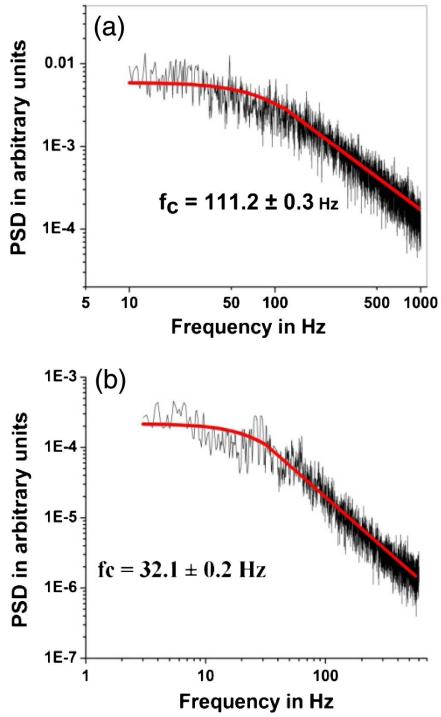

Fig. 7. PSDs extracted from the fluctuations recorded on (a) QPD*b* and (b) QPD*f* in the setup shown in Fig. 3(a).

shown in Fig. 7. It can be seen that, as in the setup using a single wavelength, the corner frequency linked to a single trapped bead resides between the corner frequencies of the PSDs recorded for the simultaneous backscattering of 1064 and 980 nm on the two QPDs. It also can be noted from the table that the corner frequency obtained from the PSD recorded on QPD*b* is higher than that recorded on QPD*f*.

C. Two Wavelength Simultaneous Forward Scattering Detection

The power spectra for a pair of trapped beads, as recorded by two wavelength simultaneous forward scattering detection, are shown in Fig. 8. Here, it can be seen that, unlike the earlier two experiments, the corner frequency extracted from the PSD analysis of the intensity fluctuations recorded on QPD*b* (forward scattering at 980 nm) is lower than that for QPD*f* (forward scattering at 1064 nm). As, for reasons outlined earlier, it is impossible that Bf experiences trap stiffness larger than that of Bb; thus, this is evidence that the fluctuation information carried by forward scattering is dominated by the bead encountered first in the optical path of the laser.

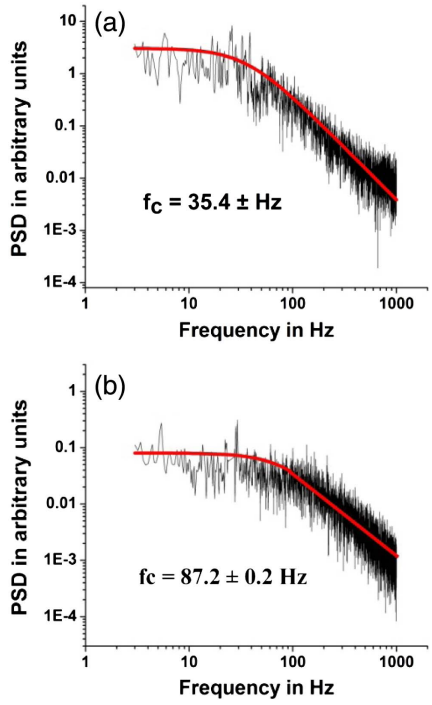

Fig. 8. PSDs extracted from the fluctuations recorded on (a) QPD*b* and (b) QPD*f* in the setup shown in Fig. 3(b).

Thus, it can be implied from the results of the above experiments that in situations of trapping of more than one bead in an optical trap, forward-scattering detection is an unreliable method for detecting the position of any of the trapped particles. It appears that detection of backscattering is a more reliable way of tracking single particle positions, but this can only be ascertained by simulation studies.

4. COMPUTER SIMULATIONS

As we have seen from the results previously discussed, when a single microscopic bead is trapped in an optical tweezer, measurements of the bead's fluctuations in both forward- and backscattering schemes yield the same information about the trap stiffness experienced by the bead. However, when two beads are trapped axially in a single-beam tweezer, the light rays collected by any detector could be scattered by both Bb and Bf (A), only by Bb (B), or only by Bf (C). Thus, any detector, whether it is aligned to the forward- or backscattering paths, will have an admixture of position information of both beads. We refer to this as cross talk. As previously mentioned, for determination of the interaction between trapped beads, one needs to obtain position information of each bead free from cross talk. Here, we describe a computation of the relative scattering intensities involving the three scenarios (A), (B), and (C), described above for forward- and backscattering schemes and show that, in the backscattering scheme, scattering of the scenario (B) is dominant.

A. Estimation of the Cross Talk in the Signal in Backscattering Measurements

As previously described, the trapped microparticles in our experiments are 3 μm polystyrene beads whose thermal

fluctuations are of the order of tens of nanometers. The trapping laser has a wavelength of 1064 nm and is focused to a circular spot of radius 0.5 μm. We, therefore, employ Mie scattering theory [9] to analyze the scattering from the trapped microbead. From this theory, the forward-scattered intensity is found to be dependent on the relative refractive index of the particle with respect to the surrounding medium and the lateral position of the microparticle with respect to the axis of the Gaussian beam. However, if the magnitudes of lateral displacements of the particle (tens of nanometers in our case) are much smaller compared with the size of the focal spot (0.5 μm in our experiments) and particle size; then, the total forward-scattered intensity will be not be strongly dependent on the particle's lateral displacements from the beam axis. To support this claim, we present results from Mie-scattering-based computation of the intensities of forward-scattered light as a function of relative position of the bead with respect to the beam axis.

From equipartition theorem, a microparticle of diameter 3 μm immersed in water at room temperature of 296 K and held in the tweezer with a corner frequency of 100 Hz has a standard deviation (σ) in its values of fluctuations of about 20 nm. For each position of the microparticle, we compute the total forward scattered light intensity collected by objective O2 [Fig. 3(a)] aligned to the forward-scattering path in order to make our simulations match the experimental arrangement. The objective O2 [Fig. 3(a)] when used with an immersion oil of index 1.52 can collect scattered light over an angle of 55.3° on either side of the central axis. Thus, we restrict our computations to within $\theta = -55.3°$ to 55.3° and $\Phi = 0°$ to 360° in the forward direction. This constitutes the angular detection range for O2. We summarize our results of forward-scattered intensity for particle fluctuations, which range from 0 to 4σ in Table 2. It may be noted that the variations in the forward-scattered intensity as a function of lateral displacement of the bead are in the fourth decimal place over this range.

From these results, we conclude that the total forward-scattered intensity of the light collected by objective O2 [Fig 3(a)] aligned to the forward-scattering path is practically invariant for the expected fluctuations of such a trapped bead (Table 2). This justifies the use of a ray-optics-based model that employs single values of reflection coefficient (R) and transmission coefficient (T) for the polystyrene beads, irrespective of the bead's lateral displacement with respect to the beam axis.

Table 2. Tabulation of the Ratio of Total Forward-Scattered Light Intensity for Lateral Displacement "d" (I) to Intensity for Zero Lateral Displacement (I_0)

Displacement "d" in Units of Standard Deviation σ	Ratio I/I_0
0.00	1.0000
0.33	1.0000
0.67	1.0000
1.00	1.0000
1.33	1.0000
1.67	1.0000
2.00	1.0000
2.33	1.0001
2.67	1.0001
3.00	1.0001
3.33	1.0001
3.67	1.0001
4.00	1.0001

In a trap where the light intensity variation is radially symmetric about the beam propagation direction, the positional fluctuations of a trapped bead, as projected onto a plane perpendicular to the beam propagation direction, is isotropic. The experimental signals obtained on any QPD can be resolved into two sets representative of orthogonal displacements of the bead. We find that a PSD-based analysis of data corresponding to orthogonal displacements of the trapped bead yield the same value for the trap stiffness. Therefore, we conclude that the trapping volume is indeed isotropic in nature, and it is sufficient to study the dynamics of the trapped bead along a single direction. Thereby, we choose to carry out our simulations in one dimension. The equation of motion for a single trapped bead in a thermal bath is represented by the Langevin equation:

$$m\frac{d^2x}{dt^2} + \gamma\frac{dx}{dt} + kx = \langle|F|\rangle\eta(t), \tag{1}$$

where the first term represents the inertial term, which can be neglected for a polystyrene microbead of 3 μm diameter suspended in double-distilled water at room temperature (300 K), $\gamma = 6\pi\eta a$ is the linear drag coefficient on a particle of radius a suspended in a liquid of viscosity η and k is the trap stiffness. The trap stiffness, k, can be written as $2\pi\gamma f_c$, where f_c is the corner frequency seen in the PSD, which is extracted from the fluctuation behavior of the trapped bead. $\langle|F|\rangle$ denotes the average magnitude of Brownian force and can be written as $\langle|F|\rangle = \sqrt{2\gamma k_B T}$ at temperature T while k_B is the Boltzmann constant. $\eta(t)$ is a random number drawn from a set of random numbers that occur with a Gaussian probability distribution about a mean of zero [10]. The Langevin equation is then solved to yield a solution that can be written as

$$x_i = \frac{C_2}{C_1} + e^{-C_1\Delta t}\left(x_{i-1} - \frac{C_2}{C_1}\right), \tag{2}$$

where x_i and x_{i-1} are two successive displacements of the trapped bead, while C_1 and C_2 are k/γ and $\eta(t) \times \sqrt{(2k_BT/\gamma)}$, respectively. The time interval Δt is chosen to be 10^{-5} s, a small fraction of k/γ, during which the Brownian force on the bead is assumed to remain constant.

Because we are treating the problem in one dimension, it is sufficient to simulate the detection mechanism considering a hypothetical two-sector detector (TSD). We assume the detector to be partitioned into two segments along a direction perpendicular to the 1D fluctuations of the trapped bead, as shown in Fig. 9. Further, we assume that the differential intensity of light falling on the two sectors of the detector is proportional to the instantaneous bead displacement. Using values of 0.9 and 0.1 for the transmission and reflection coefficient, respectively, for polystyrene as reported in [11], we obtain intensity to displacement calibration by simply dividing a set of 10^5 intensity differentials computed by the TSD simulation by corresponding displacements obtained by solving the Langevin equation iteratively.

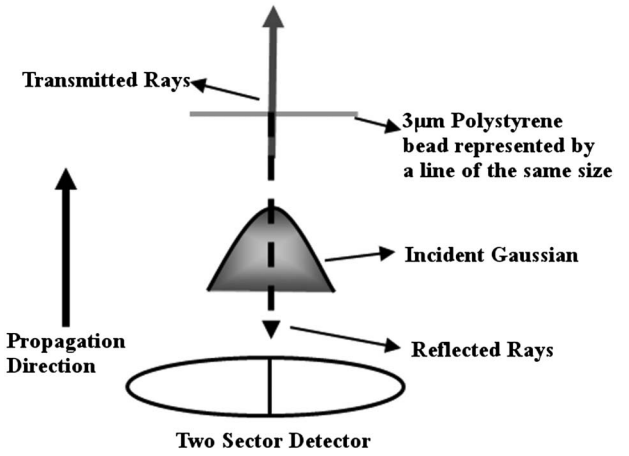

Fig. 9. Schematic of the two sector detector aligned to the path of backscattered laser light.

Whenever two beads are trapped axially in an optical trap, Bb is held more strongly compared with Bf, as Bb is closer to the focal point, according to the reasoning outlined earlier. Correspondingly, in the Langevin equation used to compute the positions of Bb, a higher trap stiffness has been assigned as compared with that for Bf. We note here that we expect to generate displacements for the individual beads using equations of the form in Eq. (1) wherein interbead interactions whether arising out of hydrodynamic-induced interbead drag, electrostatic charging or optical binding are not explicitly considered. Our assumption here is that the interbead interaction, irrespective of whether this involves conservative or dissipative forces, can still be represented by Eq. (1), albeit now with a modified trap stiffness k and drag coefficient γ. We justify this on the basis of our experiments where we find that the PSDs recorded can always be fitted to modified Lorentzians, thus indicating that the potential seen by the trapped pair of beads is still parabolic in nature. This is probably because optical binding forces are in the order of 10^{-13} N [12] and hydrodynamics-induced interbead drag is in the same order as the optical forces (10^{-12} N) [12,13], thereby making it possible to subsume these small changes into an effective interaction modified k and an effective hydrodynamics modified γ and use equations of the form Eq. (1) to represent the actual bead positions.

In order to estimate the cross talk in backscattered light (Fig. 9), we compute a simple ratio of the intensity of light scattered only from Bf to that which is scattered only from Bb (I_f/I_b) for about 50,000 values of displacements of two beads held with differing values of trap stiffness. The bead positions are generated using Eq. (1) with corner frequency, corresponding to the trap with Bb held fixed at 100 Hz while the corner frequency corresponding to the trap with Bf is varied from 10 to 90 Hz in steps of 10 Hz. In each case, we obtained a ratio of the order of 10^{-5}. The same ratio for the forward-scattering scheme ranged from 0.60 to 0.70. Thus, we conclude that backscattering yields cross-talk-free signals of the bead the laser encounters first and can always be considered a reliable method of tracking its position.

With this result from the simulations, we can gain a clearer understanding of the results of the experiments that have been described in the earlier sections. It is now evident that the simultaneous two-wavelength backscattering detection yields information with regards to the true trap stiffness experienced by each of the beads (QPDb for Bb and QPDf for Bf).

In the single-wavelength simultaneous forward- and backscattering detection, while the backscattering recorded on QPDb yields the true trap stiffness experienced by Bb, the forward scattering detected on QPDf has information of both Bb and Bf. Thus, the apparent trap stiffness extracted from a PSD analysis of the forward scattering recorded by QPDf is greater than the true trap stiffness of Bf as measured from backscattering detection because the data contains additional position information of the much more tightly held Bb.

Two wavelength simultaneous forward-scattering detection for a pair of trapped beads, on the other hand, ends up reversing the trend seen in the corner frequency magnitudes extracted from signals recorded in QPDb and QPDf.

Thus, from the results discussed so far, in a QPD-based detection scheme, a two wavelength simultaneous backscattering detection emerges as the only reliable way to monitor the positions of both trapped beads simultaneously. However, using this technique involves extensive and critical alignment of the optical components in the setup.

Single wavelength simultaneous forward- and backscattering detection is relatively easier to carry out and could be used for reliable tracking of the front particle position, if one could correct for the signal cross talk. In the next section, we present detailed results of a T-matrix-based computation of the scattered electric fields from the two axially trapped microbeads and discuss the limitations of forward-scattering detection in tracking the position of Bf.

B. Cross Talk in Forward Scattering

In the far-field limit, the pattern of light, bearing information of a trapped microbead in an OT, comprises interference between the unscattered light and scattered light and forms the basis of detection of the trapped microparticle position using a quadrant photodiode in the forward-scattering scheme [1,14,15]. Extending the situation for a single trapped bead, one may write the interference between unscattered light and that scattered by two axially trapped beads as

$$I = 0.5c\varepsilon(E_0^2 + E_b^2 + E_f^2 + 2E_0E_b + 2E_0E_f + 2E_bE_f), \quad (3)$$

where c and ε are the velocity of light in the fluid of immersion and the permittivity of the fluid of suspension, respectively. E_0, E_b, and E_f are the magnitudes of electric field corresponding to the unscattered light, light scattered from the back bead and light scattered from the front bead, respectively. Because the detection mechanism is based on the difference between unscattered and interference intensities, Eq. (3) becomes

$$\delta I = 0.5c\varepsilon(E_b^2 + E_f^2 + 2E_0E_b + 2E_0E_f + 2E_bE_f). \quad (4)$$

The trapped microbeads used in our experiments are about three times larger than the wavelength of light involved. Thereby, unlike the situations in [1] and [15], where Rayleigh scattering theory is invoked, we employ a Mie scattering

formalism along with a light intensity and wavefront description that seeks to represent the actual experimental situation of a tightly focused laser beam [14]. Because our calculations involve multiple light scattering, we have adopted the T-matrix-method-based optical tweezer toolbox (OTT) [16]. The T-matrix method has the advantage that the T-matrix linked to a scatterer has to be computed only once. Moreover, scattered light from one of the beads can be made incident on the other using the vector translation–rotation theorem-based protocols available in the toolbox.

We provide a summary of the Mie scattering formalism used for the calculations, following [16].

We represent the incident field in a series expansion of the incoming and outgoing vector spherical wave functions (VSWFs) $\boldsymbol{M}_{nm}^{(3)}(kr)$ and $\boldsymbol{N}_{nm}^{(3)}(kr)$ as

$$E_{\text{inc}}(r) = \sum_{n=1}^{\infty} \sum_{m=-n}^{n} a_{nm} \boldsymbol{M}_{nm}^{(3)}(kr) + b_{nm} \boldsymbol{N}_{nm}^{(3)}(kr), \quad (5)$$

where k is the propagation vector of the laser light in the suspension liquid.

Using the same formalism, we represent the scattered field from a single trapped microbead as

$$E_{\text{scat}}(r) = \sum_{n=1}^{\infty} \sum_{m=-n}^{n} p_{nm} \boldsymbol{M}_{nm}^{(1)}(kr) + q_{nm} \boldsymbol{N}_{nm}^{(1)}(kr), \quad (6)$$

where $\boldsymbol{M}_{nm}^{(3)}(kr)$ and $\boldsymbol{N}_{nm}^{(3)}(kr)$ [also represented as $\mathbf{Rg}M_{nm}(kr)$ and $\mathbf{Rg}N_{nm}(kr)$] are regular VSWFs and $\boldsymbol{M}_{nm}^{(1)}(kr)$ and $\boldsymbol{N}_{nm}^{(1)}(kr)$ are the vector spherical wavefunctions. Full expressions and detailed discussions of these VSWFs can be found in [16]. n and m are mode expansion coefficients. a_{nm} and b_{nm} are the expansion coefficients for the incident beam, and p_{nm} and q_{nm} are the expansion coefficients for the scattered beam. Following [17], we truncate the series expansion at a value n_{max} determined for a scatterer contained within a radius r using the expression:

$$n_{\text{max}} = kr + 3\sqrt[3]{kr}. \quad (7)$$

The T-matrix establishes a relationship between the scattered and incident beam coefficients as $p_k = \sum_n^{\infty} T_{kn} a_n$, where T_{kn} represent the elements of the T-matrix. Collecting together the terms of the column matrices for the incident and scattered beam coefficients and also the square matrix representative of the T-matrix, one can write $\mathbf{P} = \mathbf{TA}$, where P is the column matrix of the scattering expansion coefficients, T is the T-matrix, and A is the column matrix of the incident beam expansion coefficients.

Even though the pure intensity terms such as E_b^2 and E_f^2 turn out to be larger than the interference terms in a Mie scattering treatment, in an interferometric detection scheme, it is the interference terms that bear signatures of the particle position fluctuations with the pure intensity terms forming the background intensity on the detector [1,14,15].

We model a linearly polarized tightly focused Gaussian laser beam with an experimentally measured focal spot of diameter 1 μm as an LG_{00} mode using the protocols made available within the toolbox for the description of the incident field in an OT. This beam is translated to the center of Bb assuming an offset between the focus and the center of Bb. The T-matrix setup for a bead of a chosen value (0.5, 1.0, and 1.5 μm) and refractive index 1.57 suspended in water of refractive index 1.33 is applied to obtain the scattered light from Bb. We translate the scattered light from Bb to the center of Bf and apply the T-matrix again to obtain E_f, the electric field of light scattered from Bf computed in the far field [18]. Finally, the incident unscattered beam is translated from the focus to the center of Bf to obtain E_0, the electric field of unscattered light computed in the far field, and the scattered light from Bb is translated to the center of Bf to obtain E_b, the electric field of light scattered from Bb computed in the far field. These translations allow all three fields to be computed in the angular detection range detailed earlier, in the far field limit, with reference to a common starting point (i.e., the center of Bf).

While in traps comprising of two counterpropagating beams, one does expect well-defined potential minimums, which reside about a wavelength in distance from each other [4]; in our situation, we do not expect this to be the case, as we are unaware of the exact nature of the interaction between the two axially trapped microbeads. Therefore, we do not have information of the interbead separation of the trapped pair of beads [Z_e in Fig. (1)]. However, reasonable values for the distance between Bb and the laser focus along Z axis [Z_b in Fig. (1)] might be obtained by the following arguments. We obtain the axial equilibrium position of a single trapped microbead as a function of bead diameter by simply determining the zero-crossing point of the normalized axial force using the OTT [17]. We find that the axial equilibrium distances (Z_A) from the laser focus for 1, 2, and 3 μm diameter beads are, respectively, 0.32 to 0.36 μm, 0.18 to 0.20 μm, and 0.17 to 0.19 μm at a laser power coincident with experimental values. As Bb normally shows higher trap stiffness when compared with the case of single trapped bead, we posit that Z_b has to be lesser than the corresponding values of Z_A. We present here results of simulations carried out with different values of these distances (see Fig. 1). We compute the scattered fields in the far-field limit for predetermined coordinate points spread within the angular detection range of O2, as discussed earlier. Because, in an actual detection process, the detector sums the light incident on various points in a quadrant, we take a summation of different terms computed at the above-mentioned coordinate values. For example, $E_0^2 = \sum_i (E_0^2)_i$ and $E_0 E_b = \sum_i (E_0 E_b)_i$, etc., P_0, P_f, and P_b represent the power contained in the incident beam, scattered beam from Bf and scattered beam from Bb, respectively, as determined from the corresponding expansion coefficients [17].

In the results presented in Table 2, $E_f^2 > E_b^2$ for the simulations involving beads of diameter 3 μm despite the powers computed using respective beam expansion coefficients being in the order $P_0 > P_b > P_f$. This can be attributed to a buildup of double truncation error in (1) the higher-order multipoles due to translations greater than the spot size and (2) the higher-order off-diagonal terms in larger T-matrices, which come about due to the requirement of large translations [17]. For example, it can be seen that, for a pair of 1 μm diameter beads with $Z_b = 0 = Z_e$ (first row in Table 3), n_{max} is 14, and the T-matrix size is 448 × 448, whereas, for a pair of 3 μm

Table 3. Summary of Optical Tweezer Toolbox-Based Computations[a]

Bead Diameter D(μm)	n_{max}	Size of the T-Matrix	Z_b (μm)	Z_e (μm)	$E_0{}^2$	$E_b{}^2$	$E_f{}^2$	P_0	P_b	P_f	E_0E_b	E_0E_f	E_bE_f
1	14	448 × 448	0.0	0.0	215.02	15.60	2.76	0.46	0.18	0.08	−3.72	2.24	−1.02
	23	1150 × 1150	0.2	0.2	213.93	14.92	1.94	0.46	0.17	0.06	−3.17	−0.40	−0.36
	24	1248 × 1248	0.3	0.2	213.93	15.54	2.04	0.46	0.18	0.08	−1.14	−1.06	−0.37
2	24	1248 × 1248	0.0	0.0	214.22	151.41	122.56	0.46	0.42	0.37	−0.01	3.42	−109.71
	35	2590 × 2590	0.2	0.2	211.04	150.00	108.80	0.45	0.40	0.34	−1.03	−1.99	−98.83
	37	2886 × 2886	0.3	0.2	210.49	148.32	104.64	0.45	0.40	0.33	1.02	1.14	−94.12
3	24	1248 × 1248	0.0	0.0	213.80	175.73	198.52	0.46	0.41	0.38	–	–	–
	34	2448 × 2448	0.0	0.1	213.82	175.68	201.00	0.46	0.41	0.38	–	–	–

[a]Terms E_0E_b, E_0E_f, and E_bE_f have not been shown for beads of diameter 3 μm, as they correspond to unphysical electric fields (i.e., $E_f^2 > E_b^2$).

diameter beads with $Z_b = 0$ and $Z_e = 0.1$ μm, $n_{max} = 34$, and the size of the T-matrix is 2448×2448 (last row in Table 3); therefore, because of double truncation errors in both higher-order multipoles and also in the higher-order off-diagonal terms of the T-matrix, $E_f^2 > E_b^2$ for 3 μm diameter beads, which is unphysical. After checking the scattered intensities for correctness, we compute the interference between any two fields (say E_b and E_f) in the far-field limit as $E_bE_f = |E_b||E_f|(\frac{\text{real}(E_b * E_f)}{|E_b||E_f|})$, where $|E_b|$ and $|E_f|$ represents the magnitudes of the fields due to the back and front beads, respectively, and the term within the parenthesis is the phase factor. In the forward-scattering detection-based scheme in an OT, the interference between unscattered light and scattered light allows for the detection of the particle position with respect to the incident laser beam, which also defines the laboratory coordinate frame. Thus, the three interference terms shown in Eq. (3) i.e., E_0E_b, E_0E_f, and E_bE_f can be thought of as bearing position information of Bb with respect to the incident laser, position information of Bf with respect to the incident laser, and position information of Bb with respect to Bf, respectively. Therefore, if the interference term between the two scattered fields, i.e., E_bE_f were overwhelmingly smaller than the two other interference terms, then it might have been possible, in principle, to write the signal on QPDf as a linear sum of signals due only to Bb and Bf and, subsequently, correct for the cross talk in the forward scattered light and obtain true fluctuation information of Bf. However, that not being the case, this result allows us to conclude that, in order to obtain cross-talk-free fluctuation signals of two axially trapped beads using a QPD-based detection scheme, one has to carry out measurements using a two-color simultaneous backscattering scheme.

It may be noted that, thus far, the cross talk in forward scattering has been studied using the T-matrix method, whereas a ray-optics-based method is adopted to demonstrate that the backscattering is indeed cross-talk free. This has been done because our OTT is not equipped per se to handle backscattering from multiple axially trapped microspheres. In a typical simulation of backscattering from two axially trapped beads, scattered and, subsequently, forward translated beam from the first bead and the incident forward translated beam constitute the total incident field on Bf. Scattering from Bf is back-translated to the center of Bb from where, along with the scattering component due only from Bb, the fields are computed in the far-field limit. Because the total translation distance is now twice that of the forward-scattering computations, one has to use a greater number of modes (N_{max}), which increases the size of the T-matrix to be used and leads to large truncation errors in the field. Elimination of certain mode expansion terms may be able to achieve the right balance between an accurate field description while still eliminating truncation errors. This, however, involves much further careful analysis. On the other hand, alternate methods of analyzing scattered light such the angular spectrum method [19] might be able to circumvent such issues altogether.

5. CONCLUSIONS AND OUTLOOK

Through measurements of two axially trapped beads in a single-beam tweezer using forward- and backscattering techniques to obtain position information, we have demonstrated that it is not possible in single wavelength measurements to obtain information that resolves the positions of the individual beads. In particular, any measurement that relies on forward scattering is never free from cross talk and bears information dominated by the bead the laser encounters first in its propagation direction. In order to resolve this problem, we have carried out two-color simultaneous backscattering measurements. We have justified this through proof by simulation that the cross talk in backscattering is negligible. The two-color backscattering detection geometry thereby paves the way for studies on interactions between a pair of beads trapped along different axial positions in a single Gaussian beam tweezer setup. We also note that the method of detection outlined in this paper may be extended to situations wherein multiple particles are trapped axially to obtain fluctuation information of beads trapped at the extreme ends of the microbead chain.

Funding. Nano Mission Council, Department of Science and Technology (DST), government of India (SR/S5/NM-73/2006, PURSE program SR/S9/Z-23/2010/38(C)); University Grants Commission (UGC) (CPEPA project and SSI), India (F.NO.8-2/2008(NA/PE)).

Acknowledgment. The authors thank Alexander B. Stilgoe of the University of Queensland, Australia, for discussions and help with the optical tweezer toolbox and remarks on

an earlier version of the manuscript. The authors also thank Amey Joshi of Tata Consultancy Services (TCS), India, and Ayan Bannerjee of the Indian Institute of Science Education Research, Kolkata, India, for helpful discussions.

REFERENCES

1. F. Gittes and C. F. Schmidt, "Interference model for back-focal-plane displacement detection in optical tweezers," Opt. Lett. **23**, 7–9 (1998).
2. F. B. Shipley and A. R. Carter, "Back-scattered detection yields viable signals in many conditions," Opt. Express **20**, 9581–9590 (2012).
3. M. Li and J. Arlt, "Trapping multiple particles in single optical tweezers," Opt. Commun. **281**, 135–140 (2008).
4. T. Čižmár, L. C. Dávila Romero, K. Dholakia, and D. L. Andrews, "Multiple optical trapping and binding: New routes to self assembly," Phys. B **43**, 102001 (2010).
5. M. M. Burns, J.-M. Fournier, and J. A. Golovchenko, "Optical binding," Phys. Rev. Lett. **63**, 1233–1236 (1989).
6. M. M. Burns, J.-M. Fournier, and J. A. Golovchenko, "Optical matter: Crystallization and binding in intense optical fields," Science **249**, 749–754 (1990).
7. Yogesha, A. Raghu, B. V. Nagesh, S. Bhattacharya, and S. Ananthamurthy, "A dual optical tweezer for microrheology of bacterial suspensions," Int. J. Nanosci. **10**, 181–186 (2011).
8. A. Ashkin, "Forces of a single-beam gradient laser trap on a dielectric sphere in the ray optics regime," Biophys. J. **61**, 569–582 (1992).
9. C. F. Bohren and D. R. Huffman, *Absorption and Scattering of Light by Small Particles* (Wiley-Interscience, 1983).
10. G. Volpe and G. Volpe, "Simulation of a Brownian particle in an optical trap," Am. J. Phys. **81**, 224–230 (2013).
11. R. H. Boundy and R. F. Boyer, eds. *Styrene: Its Polymers, Copolymers and Derivatives*, (Reinhold, 1952).
12. S. A. Tatarkova, A. E. Carruthers, and K. Dholakia, "One-dimensional optically bound arrays of microscopic particles," Phys. Rev. Lett. **89**, 283901 (2002).
13. S. Henderson, S. Mitchell, and P. Bartlett, "Direct measurement of colloidal friction coefficients," Phys. Rev. E **64**, 061403 (2001).
14. A. Rohrbach and E. H. K. Stelzer, "Three-dimensional position detection of optically trapped dielectric particles," J. Appl. Phys. **91**, 5474–5488 (2002).
15. A. Pralle, M. Prummer, E.-L. Florin, E. H. K. Stelzer, and J. K. H. Hörber, "Three-dimensional high-resolution particle tracking for optical tweezers by forward scattered light," Microsc. Res. Tech. **44**, 378–386 (1999).
16. T. A. Nieminen, V. L. Y. Loke, A. B. Stilgoe, G. Knöner, A. M. Bránczyk, N. R. Heckenberg, and H. Rubinsztein-Dunlop, "Optical tweezers computational toolbox," J. Opt. A **9**, S196–S203 (2007).
17. User guide for optical tweezers toolbox 1.2 by A. B. Stilgoe, optical tweezer toolbox downloadable at www.physics.uq.edu.au/people/nieminen/software.html.
18. Y. Cao, L. Chen, W. Ding, F. Sun, and T. Zhu, "Optical collection of multiple spheres in single tightly focused beams," Opt. Commun. **311**, 332–337 (2013).
19. B. Roy, S. B. Pal, A. Halder, R. K. Gupta, N. Ghosh, and A. Bannerjee, "Probing the dynamics of an optically trapped particle by phase sensitive back focal plane interferometry," Opt. Express **20**, 8317–8328 (2012).